# Lattice Properties of PbX (X = S, Se, Te): Experimental Studies and *ab initio* Calculations Including Spin-Orbit Effects

A.H. Romero

*CINVESTAV, Departamento de Materiales,*

*Unidad Querétaro, Querétaro, 76230, Mexico*

M. Cardona, R. K. Kremer,* R. Lauck, and G. Siegle

*Max-Planck-Institut für Festkörperforschung,*

*Heisenbergstr. 1, D-70569 Stuttgart, Germany*

J. Serrano

*ICREA-Dept. Física Aplicada, EPSC,*

*Universitat Politécnica de Catalunya,*

*Av. Canal Olímpic 15, 08860 Castelldefels, Spain*

X. C. Gonze

*Unité de Physico-Chimie et de Physique des*

*Matériaux Université Catholique de Louvain*

*B-1348 Louvain-la-Neuve, Belgium*

(Dated: August 25, 2008)

## Abstract

During the past five years the low temperature heat capacity of simple semiconductors and insulators has received renewed attention. Of particular interest has been its dependence on isotopic masses and the effect of spin- orbit coupling in *ab initio* calculations. Here we concentrate on the lead chalcogenides PbS, PbSe and PbTe. These materials, with rock salt structure, have different natural isotopes for both cations and anions, a fact that allows a systematic experimental and theoretical study of isotopic effects e.g. on the specific heat. Also, the large spin-orbit splitting of the $6p$ electrons of Pb and the $5p$ of Te allows, using a computer code which includes spin-orbit interaction, an investigation of the effect of this interaction on the phonon dispersion relations and the temperature dependence of the specific heat and on the lattice parameter. It is shown that agreement between measurements and calculations significantly improves when spin-orbit interaction is included.

# I.  INTRODUCTION

Considerable effort has been spent recently in the investigation of the heat capacity $C$ of semiconductors and insulators in the region below the Debye temperature $\theta_D$ , in particular around 0.1 $\theta_D$ , where strong deviations from Debye's $T^3$ power law take place. The availability of stable isotopes has also enabled the investigation of the dependence of $C$ on one isotopic mass (in monatomic crystals such as C (Ref. 1), Si (Ref. 2), Ge (Ref. 3,4), Sb (Ref. 5), Bi (Ref. 6)) or on the isotopic mass of each constituent in polyatomic compounds, such as GaN (Ref. 7) or Zn0 (Ref. 8), whereas the development of efficient computer codes for electronic band structure calculations has made possible *ab initio* calculations of the phonon dispersion relations and the temperature dependence of the specific heat.

Although experimental and calculated results for $C_v \approx C_p$ (Ref. 9) agree usually reasonable well, it has been recently discovered that considerable discrepancies exist when heavy constituent atoms are present, e.g. Bi (Ref. 6), Pb in PbS (Ref. 9), if the Hamiltonian used for the calculation of the electronic structure does not include spin-orbit (s-o) interaction. By performing *ab initio* calculations in which the s-o interaction is switched on and off, it has been rather conclusively shown that this interaction "softens" the phonon frequencies (Ref. 10,11) and thus increases the low-temperature maximum found in $C_v/T^3$ versus $T$.[6]

In this article we present *ab initio* calculations of the phonon dispersion relations of PbS, PbSe and PbTe based on the electronic band structure obtained with the ABINIT code.[12] This program enables the inclusion of s-o interaction, separately or jointly for the cation or anion constituents, thus making it possible to separate the s-o contributions to the dispersion relation and the heat capacity. The ABINIT program determines the dynamical matrix elements by perturbation theory. Once these elements are known, it is a simple task to calculate the dispersion relations for a given set of isotopic masses and thus to determine isotopic effects on the dispersion relations and the specific heat. Because of the importance of s-o interaction, we have performed the isotope effect calculations only with s-o interaction included. Within the range of stable isotopes available in nature (and accessible to our budget) only mass changes of a few percent are possible: the resulting variations in the physical properties are thus linear in the mass changes. Results for PbS have already been published in Ref.9. At that time, the ABINIT code did not properly include s-o interaction for diatomic polar compounds. We therefore present here similar results including

s-o interaction: the inclusion of this interaction reduces the discrepancy between calculated and experimental values of $C_{v,p}$ (29%) by a factor of 2. A similar reduction is found for PbSe, whereas for PbTe the calculated values almost exactly agree with the measured data. In this latter case the effect of the s-o interaction on the maximum of $C_v/T^3$ is 18% (we recall that the s-o interaction softens the phonons and correspondingly increases $C_v/T^3$ at the maximum). Globally, the inclusion of s-o interaction also improves the agreement between the calculated and the measured (by inelastic neutron scattering, INS) phonon dispersion relation, except for the LO phonons in the vicinity of the $\Gamma$-point of the Brillouin zone (BZ). At this point, the long range electric fields associated with the LO phonons lead to some convergence problems which we have not been able to avoid completely.

In Ref. 9, and in Ref. 13 we also reported densities of one- and two-phonon (with the same $k$-value both, as required to compare with optical spectroscopy results) states, calculated for PbS in the absence of s-o interaction. We present here similar two-phonon spectra obtained for the three lead chalcogenides including s-o interaction. The features obtained in the density of one-phonon states, and their projections on the constituent atoms, are useful (and very instructive) for the interpretation of the isotope effects.

We have also looked at the effect of s-o interaction on the lattice parameter $a_0$ as obtained by energy minimization. This effect is rather small ($\sim 0.2\%$). It does not help to reduce the discrepancy between the calculated and the measured values, which is about 2%.

## II.   THEORETICAL DETAILS

The calculations of the dispersion relations and the specific heat were performed with the dynamical matrix obtained from the LDA electronic structure calculations using the ABINIT code.[12] Hartwigsen-Goedecker-Hutter relativistic separable dual-space pseudopotentials were used.[14] We performed checks with LDA and GGA functionals and convinced ourselves that no significant differences resulted; we therefore used LDA functionals throughout. For the Pb pseudopotential we also checked that our conclusions did not depend on the inclusion of $5d$ electrons in the valence bands. This allows us to use the pseudopotential as it is given in the ABINIT website. The implementation of the s-o term has been discussed in Ref. 11. We investigated cell parameter convergence as a function of energy cutoff and $k$-grid mesh. With the cutoff at 60 Hartree the total energy is converged up to 0.5 meV and stresses

are lower than 0.006 GPa. The BZ is sampled using a 6 × 6 × 6 Monkhorst-Pack grid.[15] Technical details of the calculations of the phonon dispersion relations can be found in Ref. 16 and 17. Prior to obtaining the dynamical matrix the lattice parameter $a_0$ was optimized through minimization of the total energy. In the calculations we used this parameter and not the experimental one.

After obtaining the dispersion relations, the phonon free energy $F$ was calculated with the integral given in Eq. (2) of Ref. 9. The specific heat was obtained with the expression:

$$C_v = -T \left( \frac{\partial^2 F}{\partial T^2} \right)_v. \tag{1}$$

After calculating the dynamical matrix elements we diagonalized the Hamiltonian for two different sets of masses (either cation or anion) differing by about 5%. The resulting dispersion relations were then used to calculate the derivatives of $C_v$ with respect to either mass. The logarithmic derivatives were also calculated because they can be related to the corresponding derivative with respect to temperature. The appropriate relation is given in Eq. (4) of Ref. 9 for the case of a monatomic crystal. For diatomic crystals such relation is not as simple since both, derivatives of $C_v$ versus the masses of cation and anion must be added in order to obtain the temperature derivative:

$$\frac{d\ln(C_{p,v}/T^3)}{d\ln M_{\text{Pb}}} + \frac{d\ln(C_{p,v}/T^3)}{d\ln M_{\text{X}}} = \frac{1}{2} \left( 3 + \frac{d\ln(C_{p,v}/T^3)}{d\ln T} \right). \tag{2}$$

where X = S, Se or Te, respectively.

When calculating numerically the derivatives above at very low temperatures ($\leq$ 5K) one encounters a convergence problem because of the small values of $C_v$ and $T$. Fortunately, the limit $T \to 0$ can be obtained analytically by using the Debye-$T^3$ approximation. The corresponding expressions are found in Eq. (5) of Ref. 9.

## III.   EXPERIMENTAL PROCEDURE

Samples of PbX (X = S, Se, Te) were prepared by first reacting the corresponding pure elements and then subliming the product in an argon atmosphere.

In order to purify the lead isotope oxide layers on the metal pieces were removed by etching in diluted nitric acid and, in the case of natural lead, by cutting. Subsequently, the pieces were melted in silica ampoules in hydrogen or argon. Remaining oxide stuck to the

ampoule wall after rocking and rolling the droplets at temperatures from 400 to 650$^o$C. The chalcogens were purified by sublimation and separation of the ampoule portion containing the residues. In the case of $^{130}$Te, we first reduced $^{130}$TeO with sulfur.[18] The synthesis was performed in argon by increasing the temperature to ∼650 $^o$C of the chalcogen. In the sealed silica ampoule crystal growth took place by sublimation at temperatures of 750 to 850 $^o$C under excess of the corresponding chalcogen. This resulted in a cabbage-like growth of the compound on the lead. A few platelets up to 4 × 4 mm$^2$ were obtained during 1 to 2 weeks.[19] The preparation and some properties of the PbS samples are described in some of the measured PbS samples were natural galena crystals.[20]

The heat capacities were measured between 2 and 280K with a PPMS system (Quantum Design, 6325 Lusk Boulevard, San Diego, CA.) as described in detail Ref. 8.

We also measured natural galena crystals.

## IV. DISPERSION RELATIONS

The phonon dispersion relations calculated along three high symmetry directions of the BZ ( [111], [100], [011]) for PbS are shown in Fig. 1 together with INS data of Elcombe.[21] The calculations without s-o coupling were already published in Ref. 9. Note that the s-o interaction lowers all phonon frequencies, bringing the calculations in better agreement with the experiments except for the LO band where, on the average, the agreement is similar. As we shall see later, the decrease in the calculated frequencies raises he maximum in $C_v/T^3$ , thus improving agreement with experimental data.

Figure 2 and 3 display the dispersion relations of PbSe and PbTe respectively, calculated with and without s-o coupling, together with experimental data. For both materials we also observe the decrease of phonon frequencies when the s-o interaction is taken into account. For PbSe only few experimental (INS) data points are available.[22] Figure 2 provides some indication that also in this case the calculations with s-o coupling come closer to the experimental data than those without.

Figure 3 shows calculated (with and without s-o interaction) and measured (by INS at 297K) phonon dispersion relations of PbTe. Again we observe a lowering of nearly all frequencies induced by taking into account s-o interaction, which also brings the calculations, in most cases, closer to the experimental data. The measured TO frequencies are known to
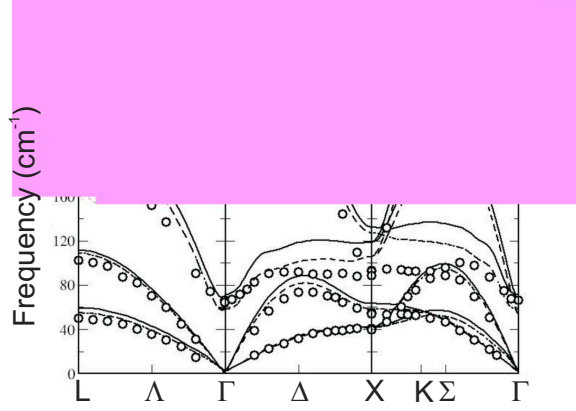
6

FIG. 1: Phonon dispersion relations of PbS with natural isotope composition of Pb and S calculated with and without s-o splitting within the harmonic approximation. The points were obtained by INS at 300 K (From Ref. 21). Typically, anharmonic effects should have lowered them by $\sim 2$ cm$^{-1}$.

be strongly renormalized downwards by the anharmonic interaction, even at low temperatures. By linearly extrapolating to $T$=0 the measured dependence of the TO frequency on temperature (from Ref. 25) we obtain an unrenormalized (harmonic) TO frequency of $\sim$13 cm$^{-1}$, rather close to that calculated with s-o interaction ($\sim 14$ cm$^{-1}$, cf. Fig.3). This low TO frequency for $T \sim 0$K underscores the nearly ferroelectric nature of this material which would nominally become ferroelectric at $\sim$-70K.[25]

A disturbing feature of Fig 3 is the dip in the LO-phonon band around the $\Gamma$- point when s-o coupling is taken into account. We have been able to show that the appearance of this dip is related to the closing and sign reversal of the electronic gap induced by the s-o splitting of the valence and conduction band edges. Lowering the s-o Hamiltonian by multiplication by an adjustable parameter $\lambda \leq 1$ (cf. Ref. 6, see also Sect. IV) the electronic gap of PbTe decreases from 0.32 eV for $\lambda = 1$, becomes zero at $\lambda \sim 0.75$ rising again to 0.53 eV for $\lambda =$
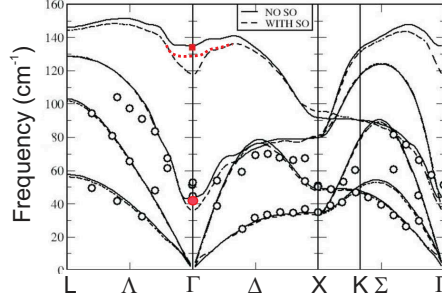
FIG. 2: (color online) Phonon dispersion relations of PbSe with natural isotope composition of Pb and Se calculated with and without s-o splitting within the harmonic approximation. The circles (○) were obtained by INS at 300 K (From Ref. 22). The (red) square was obtained by tunnel spectroscopy at 4.2 K.[23] Typically, anharmonic effects should have lowered them by $\sim 2$ cm$^{-1}$. The (red) closed circle was obtained by ir transmission at 1.4K.[24] The (red) dotted line isuggests how the LO band should look like (for more details see text).

0 (the value of the gap measured at 4 K is 0.19 eV (Ref. 27). Note that for PbSe (Fig.2) a similar but smaller dip occurs when the s-o interaction is switched on. In this case, the band gap nearly vanishes for $\lambda = 0$ and becomes 0.52 eV for $\lambda = 1$, with the same inverted order as in PbTe. Reversal of the gap is smaller than for PbTe because the s-o splitting of Se is smaller than that of Te. For PbS (cf. Fig. 1) no dip is present other than that already existed without s-o splitting. The gap is $\sim 0$ for $\lambda = 0$ and 0.47 eV (also inverted) for $\lambda = 1$.

In view of the systematics of the effects just described we conjecture that the anomalous dip in the LO frequencies observed at the $\Gamma$-point, is due to electron-phonon interaction of the type named after Kristoffel and Konsin.[28] This interaction lowers the phonon frequencies at $\Gamma$ and can even lead to ferroelectricity when a phonon frequency vanishes (this is almost
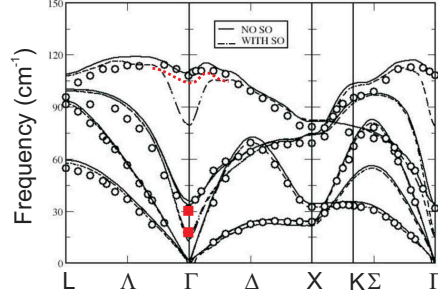
FIG. 3: (color online) Phonon dispersion relations of PbTe with natural isotope composition of Pb and Te calculated with and without s-o splitting within the harmonic approximation. The (black) circles were obtained by INS at 297 K (From Ref. 26). The (red) squares were obtained by optical spectroscopy at 300K ($32$ cm$^{-1}$) and 5K ($18$ cm$^{-1}$).[25] The (red) dotted line suggests how the LO band should look like (for more details see text)

but not quite the case for PbTe but happens for SnTe, for which the gap is reversed with respect to PbTe.[29,30] Since the measured LO frequency does not support the presence of the dip calculated for PbTe (and also less strongly for PbSe) we conclude that the dip is due to some as yet unidentified effect of the s-o interaction, probably related to the gap anomalies just described (and to the so-called gap problem ubiquitous in LDA calculations). We have just made a guess as to how the LO band should look like once the problem is removed, and represented it by a dotted red line, for both PbTe and PbSe (cf. Fig. 2 and 3). Because of the small volume of $k$-space encompassed by the dip ($\sim 0.1\%$ of the BZ) we believe that this problem should not affect our calculations of heat capacities.

## V.  PHONON DENSITIES OF STATES AND RAMAN SPECTRA

The densities (DOS) of one-phonon states for the three materials under consideration are displayed in Fig. 4, normalized to 6 states, as corresponds to one primitive cell (PC). This figure shows not only the total DOS but also its projection onto each of the two constituent atoms. A DOS calculated using the dispersion relations without s-o interaction has already been reported for PbS in Ref. 9. Here we report only the calculations performed with s-o interaction.

A comparison of the results in Fig. 4 for PbS with those in Fig. 2 of Ref. 9 (no s-o interaction) clearly shows the shrinking of the width of the phonon bands, from 250 cm$^{-1}$ without s-o to $\sim$ 235 cm$^{-1}$ produced by the s-o interaction. Also, whereas without s-o interaction the vibrations of the two constituents are almost fully separated in frequency (dividing line 112 cm$^{-1}$), this is not the case any more if s-o coupling is included. As shown in Fig. 4 for PbS both types of vibrations (Pb-like and S-like) overlap in the region between 100 and 130 cm$^{-1}$, presumably related to the shrinking of the phonon band width. In the case of PbSe three bands are seen in Fig. 4. The low frequency one, with a strong peak at $\sim$ 50 cm$^{-1}$, corresponds to Pb-like vibrations of TA phonons, whereas the high frequency one, centered at about 125 cm$^{-1}$, is LO- and TO- like and encompasses almost exclusively (95%) Se vibrations. The third band, centered around 80 cm$^{-1}$, is a mixture of LA- and TO- like modes and encompasses vibrations of both constituent atoms with nearly the same amplitude. The DOS of PbTe also exhibits 3 bands with a "pseudogap" at 60 cm$^{-1}$ and a second, not as deep, at $\sim$ 85 cm$^{-1}$ .The lower band, mainly TA-like with some TO and LA contribution, is predominantly Pb-like, whereas the middle band is about 66% Te-like and 33% Pb-like. These facts, which will be useful when we discuss the dependence of the heat capacity on isotopic mass, are quantitatively represented in Fig. 4 (right vignette) which displays the integrated total number of states and their projections, as a function of frequency. The integrated (total) phonon states of PbS show clearly the almost complete separation of Pb and S vibration, below 115 cm$^{-1}$ Pb-like, above S-like, and the existence of a central band of mixed modes in PbSe and PbTe.

Beside the one-phonon DOS just described, we have also calculated the DOS of two-phonon states with total zero wave vector (or, equivalently, equal wave vectors). These DOS are useful for the interpretation of second order Raman scattering since first order Raman
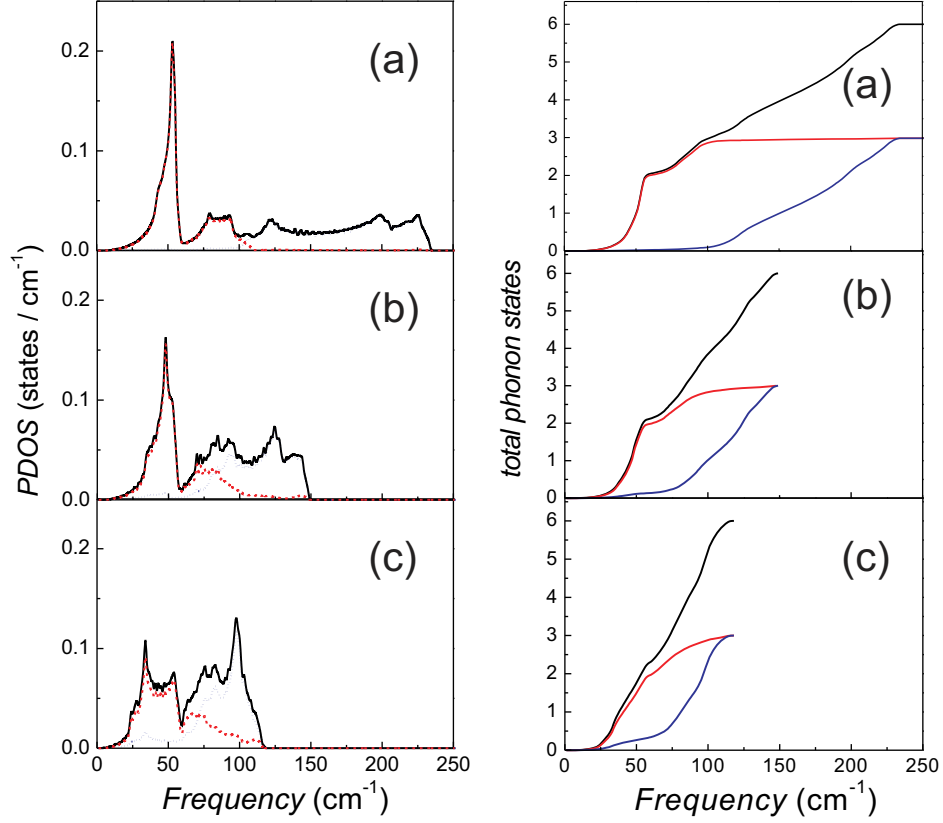
FIG. 4: (color online) (left) (a-c) Phonon density of states PDOS of PbS, PbSe and PbTe, from top to bottom, respectively. The projections of the PDOS on the two constituents is shown by the dashed lines. red: Pb projection; blue: projection on S, Se and Te, respectively. (right) (a-c) Integrated PDOS (solid black line) showing the total number of states and their projections on the cation (red line) and the anion (blue line) constituents.
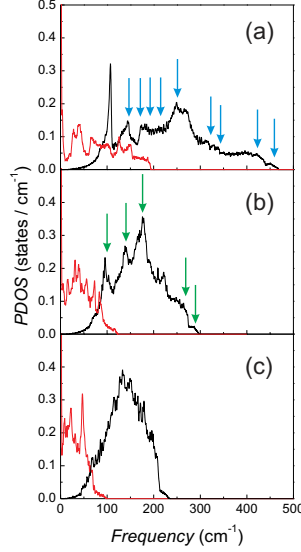
FIG. 5: (color online) (a-c) Densities of two-phonon states (sum and difference) for PbS, PbSe, and PbTe, from top to bottom respectively, with zero total $k$-vector. Notice that for the sums the curves are normalized to 36 states (6×6 states per PC). For the differences they are normalized to 15 states (6×5/2 staes per PC). The blue arrows mark structure which is weakly (except for strong 430 - 460 cm$^{-1}$peaks) observed in the Raman spectrum of PbS [ at $\sim$ 150, 180, 205, 220, 250, 320, 340, 430, 460 cm$^{-1}$].[13] The green arrows indicate possible structure related to the spectra published in Refs. 31 and 32 for PbSe.

scattering is forbidden, cf. Ref. 13. Two kinds of second order processes are possible, one in which the frequencies of the two phonons add (sum processes) and the other in which they subtract (difference processes). We calculate the DOS for both. In Raman scattering sum processes are present even at $T$=0 and increase with increasing temperature according to the appropriate statistical factors. Difference processes have vanishing intensity at $T$=0 and can only be observed with increasing temperature. We display in Fig. 5 the densities of two-phonon states for such sum and difference processes. Note that they are normalized to 36 states (6×6 states per PC) for the former and to 15 states (6×5/2) for the latter, the factor of 2 corresponding to the separation of Stokes and anti-Stokes spectra. The blue arrows

mark structure which is weakly observed (except for the strong 430 - 460 cm$^{-1}$ peaks) in the Raman spectrum of PbS [ at $\sim$ 150, 180, 200, 220, 250, 320, 340, 430, 460 cm$^{-1}$].[13] The green arrows indicate possible structure related to the spectra published in Refs. 31 and 32 for PbSe. No structure has been identified as corresponding to phonon differences, although the band seen in Fig. 5 at $\sim$ 40 cm$^{-1}$ , which seems to correspond to differences of TO and LA phonons (see Fig. 1), should increase strongly with temperature and be identifiable with a good spectrometer that covers, with little straight light, the corresponding region.

Second order Raman spectra of PbSe and PbTe are rather scarce in the literature. Some data are available for PbSe films grown on BaF$_2$ (Ref. 31) and for bulk PbSe (Ref. 32) with a small amount of Sn replacing Pb. A doublet is observed at 265 - 300 cm$^{-1}$ which corresponds to structure in the sum spectrum of Fig. 5 (see (green) arrows) an is rather similar to the doublet described above for PbS (430 - 460 cm$^{-1}$). The (green) arrows at 100, 135, 175, 265 and 290 cm$^{-1}$ also correspond to structure seen in the experimental spectra, although it is not clear whether the 135cm$^{-1}$ structure is due to scattering by two phonons or forbidden scattering by one LO phonon.[13] A peak is also observed in the measured spectra at $\sim$ 90 cm$^{-1}$ (Ref. 31). It has been attributed by the authors of Ref. 31 to difference scattering (LO-TO) although, according to Fig.5, it could also be related to the peak in the sum DOS. Without measurements of the temperature dependence of this peak it is not possible to clarify the assignment. The Raman data available for PbTe seem to be of poor quality because of segregation at the surface of TeO$_2$ and other compounds: The only structure that is clearly identifiable corresponds to a single LO phonon ($\sim$120 cm$^{-1}$).[33]

## VI. HEAT CAPACITIES

Figure 6 displays the heat capacities of PbX (X = S, Se, Te) with the natural isotope composition on either constituent. For comparison, also literature data are shown. We have chosen to plot the measured $C_p$ (and the calculated $C_v$ ) so as to be able to read the data from the plots above $\sim$ 50 K with some accuracy. Below $\sim$ 50 K the heat capacities become rather small and it is more convenient to plot $C_{p,v}/T^3$, as will be done in the subsequent figure. Notice that at the highest temperatures in Fig. 6, the heat capacities tend to the Petit-Dulong limit ( $\sim$50 J/mol K). The agreement between experimental and calculated results is excellent although it is not possible, in these plots, to see the advantage of using

in the calculations a Hamiltonian with s-o interaction. Such advantage only appears below 50 K, especially in the region where $C_p/T^3$ has a maximum.
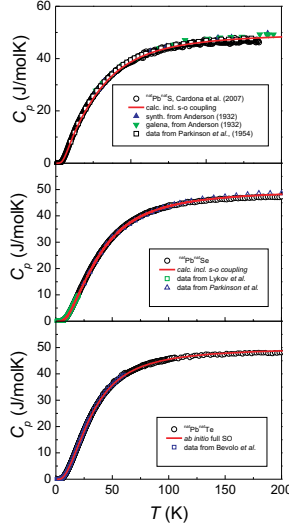


FIG. 6: (color online) Temperature dependence of the heat capacities of PbX (X=S, Se, Te) from top to bottom, respectively measured by us and other authors. The results of our *ab initio* calculations, which include s-o interaction, are shown by (blue) solid lines. Literature data have been taken from Refs. 35,36,37,38, as indicated.

Figure 7 displays the temperature dependence of $C_{v,p}/T^3$ as measured in the 2 - 60 K range and calculated with and without s-o interaction for PbS and PbSe, all constituents with the natural isotope abundance. The data for PbS are identical to those published in Ref. 9.

It is of interest to compare the effect of the s-o interaction on the calculations of Fig. 7 with that found for bismuth (Ref. 6) which has a s-o interaction similar to that of lead. The maximum in $C_v/T^3$ calculated for Bi without s-o interation is 20% below the measured one. Inclusion of s-o interaction yields a maximum 7% higher than the measured one, i.e., 27% higher than that calculated without s-o interaction.[6] The strong s-o effect calculated for Bi may result from the fact that there are two equal atoms per PC of Bi whereas for the lead

14

chacogenides there is only one heavy atom (Pb) per PC.

Figure 7(b) displays $C_p/T^3$ as measured for three samples of PbSe with different isotopic compositions, together with three curves for $C_v/T^3$ calculated with different contributions of the s-o interaction and with no s-o interaction. The purpose of this exercise was to identify the separate effects of the s-o interactions of Pb (atomic s-o splitting of the $6p$ electrons $\Delta_{\mathrm{Pb}}$= 1.27 eV) and Se ($\Delta_{\mathrm{Se}}$ =0.42 eV (Ref. 34)). The calculations in Fig. 7(b) correspond to full s-o interaction, interaction only for Pb and interaction only for Se. Notice that the calculation with only the s-o coupling of Se is rather close to that with no s-o coupling at all. The s-o effect on $C_v$ is roughly proportional to the square of the s-o coupling parameter (cf. Ref. 6) which for the valence electrons of Pb is three times bigger than that of Se. Hence, the effect of the s-o of Se alone is expected to be $\sim$ 10 times smaller than that of Pb, i.e. unnoticeable in Figure 7. However, $C_v/T^3$ with s-o coupling for both constituents is slightly larger ($\sim$3%) than if only the s-o interaction of Pb is included. This suggests the presence of bilinear terms in the corresponding perturbation expression. In order to quantify these effects we define three partial contributions $c_{\mathrm{Pb}}$ , $c_{\mathrm{Se}}$ and $c_{\mathrm{Pb-Se}}$, which represent the contribution to the s-o effect quadratic in the s-o of Pb, in that of Te, and the bilinear contribution. A fit of these effects on $C_v/T^3$ shown in Fig. 7(b) yields:

$$c_{\mathrm{Pb}} = 99.6\mu\mathrm{J/molK}^4, c_{\mathrm{Se}} \sim -3\mu\mathrm{J/molK}^4, c_{\mathrm{Pb-Se}} = 76.2\mu\mathrm{J/molK}^4 \qquad (3)$$

Obviously, the bilinear term $c_{\mathrm{Pb-Se}}$ plays a rather important role in the perturbation expansion, almost as important as the quadratic term. This suggests the detailed investigation of a material with a larger s-o coupling for the anion, such as PbTe ($\Delta_{\mathrm{Te}}$ =0.86 eV, Ref. 34). The temperature dependence of $C_p/T^3$ measured for samples with several isotopic compositions in the 3 - 14 K region, where the maximum occurs, is shown in Fig. 8. As already suspected, bilinear effects are large. They can be elucidated by multiplying the s-o Hamiltonian corresponding to the two constituents by two parameters $\lambda_{\mathrm{Pb}}$ and $\lambda_{\mathrm{Te}}$, respectively. Full s-o interaction is obtained for $\lambda_{\mathrm{Pb}} = \lambda_{\mathrm{Te}}$= +1. Information about bilinear (and also cubic, cf. Ref. 6) terms is readily obtained by reversing the sign of one of either $\lambda_{\mathrm{Pb}}$ or $\lambda_{\mathrm{Te}}$ . Additional information concerning the perturbation expansion of $C_p/T^3$ versus s-o interaction is obtained by setting one of either $\lambda_{\mathrm{Pb}}$ or $\lambda_{\mathrm{Te}}$ equal to zero, the other equal to one.

Figure 8 shows the experimental points for $C_p/T^3$ of PbTe obtained with the isotopic
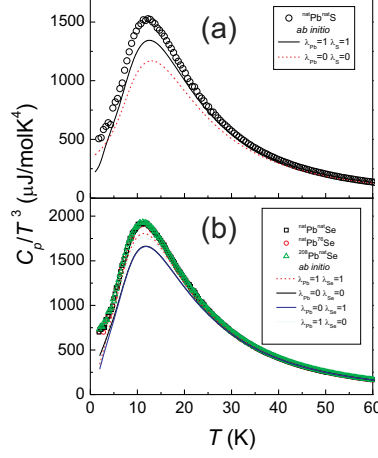
FIG. 7: (color online) (a) Heat capacity of PbS divided by $T^3$. The (black) circles represent our experimental data (from Ref. 9). The (black) solid lines represents the *ab initio* calculations with s-o interaction for Pb and S, respectively ($\lambda_{Pb}=\lambda_S=1$). The red (dashed) line represents the *ab initio* calculation with s-o interaction left out ($\lambda_{Pb}=\lambda_S=0$). Note that for the calculations without s-o the maximum lies 27 % below the measured one. Inclusion of s-o interaction reduces the discrepancy by a factor of two. For the three curves (experimental and *ab initio*) the maxima occur at $\sim$12.5 K. (b) Measured $C_p/T^3$ for three PbSe samples with different isotopic compositions as explained in the inset. The heat capacities of the three samples with different isotope composition are almost indistinguishable. The results of the *ab initio* calculations are represented by the (red) dashed, the (green) dotted and the (blue) and (black) solid lines, the latter two are almost indistinguishable, i. e. the effect of s-o interaction of only Se is not noticeable, while there is a significant increase near the maximum of $C_p/T^3$ ($T_{max} \sim 11.3$ K) if s-o interaction for Pb is taken into account ((red) dashed and green (dotted) lines. For more details see inset).

16

compositions given in the inset. The vertical scale is not wide enough to see differences for the various isotopes: such differences will be discussed later. The experimental maximum occurs at $\sim 8.5$ K, nearly independently of isotopic composition. In order to check the separate effects of $\Delta_{\mathrm{Pb}}$ and $\Delta_{\mathrm{Te}}$ on the *ab initio* calculations of $C_v/T^3$ we have multiplied the s-o interaction of Pb and Te by $\lambda_{\mathrm{Pb}}$ and $\lambda_{\mathrm{Te}}$ , respectively. We have then performed calculations for the six (after subtracting $\lambda_{\mathrm{Pb}} = \lambda_{\mathrm{Te}} = 0$) sets of values of these separate parameters, as was done in the case of bismuth in Ref.6 (only for a single $\lambda$ corresponding to bismuth, since there we dealt with a monatomic crystal). The seven sets of values of $\lambda_{\mathrm{Pb}}$ and $\lambda_{\mathrm{Te}}$ used, also given in the inset of Fig. 8, are: (1,1), (1,-1), (-1,1), (-1,0) , (1,0), (-1,-1) and (0,0) for ($\lambda_{\mathrm{Pb}}, \lambda_{\mathrm{Te}}$). We have fitted the values of $C_v/T^3$ at 9K (the vertical line in Fig. 8), after subtraction of the value for $\lambda_{\mathrm{Pb}} = \lambda_{\mathrm{Te}}) = 0$ (i.e., without s-o interaction for both constituents) to four parameters chosen as follows:

$$C_v/T^3(\lambda_{\mathrm{Pb}}, \lambda_{\mathrm{Te}}) - C_v/T^3(\lambda_{\mathrm{Pb}} = 0, \lambda_{\mathrm{Te}} = 0) = \lambda_{\mathrm{Pb}}^2 c_1 + \lambda_{\mathrm{Te}}^2 c_2 + \lambda_{\mathrm{Pb}}\lambda_{\mathrm{Te}} c_3 + \lambda_{\mathrm{Pb}}^3 c_4 \quad (4)$$

With five calculated values of Eq.(4) and four fitting parameters the corresponding values of $c_i$ are overdetermined and only an approximate fit is expected.

By minimizing the corresponding variance we find the values of $c_i$ given in Table I together with the calculated values of $C_v/T^3$ ($\lambda_{\mathrm{Pb}}$ ,$\lambda_{\mathrm{Te}}$) and the fitted ones. The fit with four parameters of the five data seems to be reasonable and thus the perturbation expansion of Eq.(4) is acceptable. Like in the case of PbSe discussed above, the quadratic term $c_1$ is close to the bilinear one $c_3$ . Also like in the case of Bi, with a s-o $6p$ splitting similar to that of Pb (Ref. 34), a cubic term is needed to represent the calculated results.[6]

## VII.   DEPENDENCE OF THE HEAT CAPACITIES ON THE ISOTOPIC MASS

The derivatives of $C_{v,p}/T^3$ with respect to the isotopic masses of either Pb or S in PbS have been presented in Ref. 9, obtained experimentally and by *ab initio* calculations. Although the calculations were performed without s-o coupling, the scatter of the experimental data, due to the small range of isotopic masses available, does not warrant a repetition of the calculations with s-o coupling. We shall present here similar results for PbSe and PbTe, with the *ab initio* calculations including s-o interaction. Figure 9 displays the results obtained
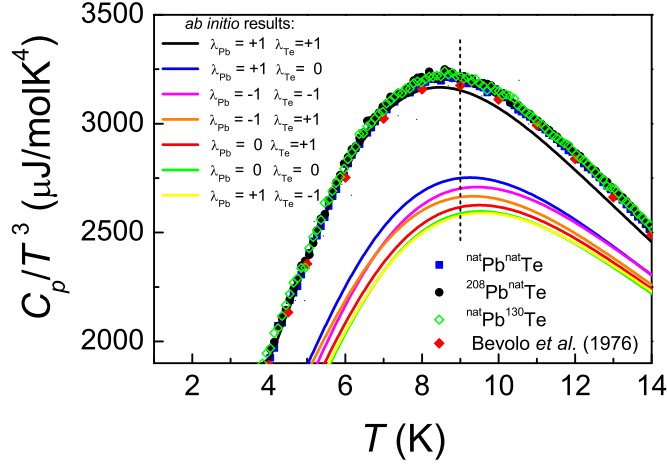
FIG. 8: (color online) (a) Heat capacity of PbTe divided by $T^3$. The symbols represent our experimental data for various isotope compositions (cf. lower inset). The (black) solid line represents the *ab initio* calculations with s-o interaction for Pb and Te, respectively ($\lambda_{\mathrm{Pb}}=\lambda_{\mathrm{Te}}=1$). The (colored) solid lines represent the *ab initio* calculations with various combinations of the s-o interaction included (cf. upper inset, from top to bottom in the same order as in the figure). Literature data have been taken from Ref. 38), as indicated.

TABLE I: Expansion, $c_1\lambda_{Pb}^2 + c_2\lambda_{Te}^2 + c_3\lambda_{Pb}\lambda_{Te} + c_4\lambda_{Pb}^3$ used to quantify the contributions to the quantity $C_p/T^3(9\mathrm{K})$ if s-o coupling for either Pb ($\lambda_{Pb}=1$) or Te ($\lambda_{Te}=1$) is taken or not taken ($\lambda_{Pb}=\lambda_{Te}=0$) into account (cf. Eq. (4)). The values of the coefficients $c_i$ that optimally fit the data are: $c_1$=247.5$\mu$ J/molK$^4$, $c_2$=64.2$\mu$ J/molK$^4$, $c_3$=287.25$\mu$ J/molK$^4$, and $c_4$=-50.62$\mu$ J/molK$^4$.

| $c_1\lambda_{Pb}^2 + c_2\lambda_{Te}^2 +$ $c_3\lambda_{Pb}\lambda_{Te} + c_4\lambda_{Pb}^3$ | $\Delta C_p/T^3(9\mathrm{K})\,(\mu$ J/molK$^4$) | |
|---|---|---|
| | calcul. | experim. |
| $c_1 + c_2 + c_3 + c_4$ | 548.3 | 565.7 |
| $c_1 + c_4$ | 196.9 | 162.0 |
| $c_2$ | 64.2 | 29.3 |
| $c_1 + c_2 - c_3 + c_4$ | -26.2 | -8.8 |
| $c_1 + c_2 - c_3 - c_4$ | 75.0 | 75.0 |

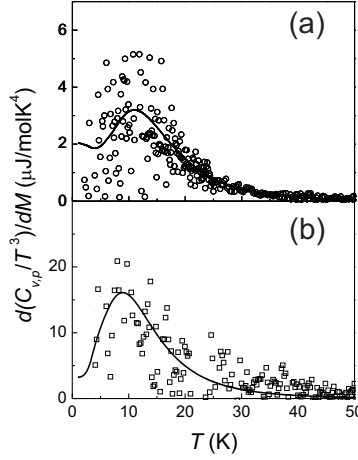for PbSe using the isotopic samples given in the inset.



FIG. 9: Derivatives of $C_{v,p}/T^3$ of PbSe with respect to the isotopic masses of (a) Pb and (b) Se as measured using samples of different isotopic compositions, compared with *ab initio* calculations for various isotope masses with s-o interaction included.

A model for relating the position in the maxima of Figs. 9 and 10 was presented in Ref. 9. It made use of a single Einstein oscillator to represent prominent peaks in the one-phonon DOS (Fig. 4). The peak of the mass derivatives (Figs. 9 and 10) takes place at the Einstein frequency (converted into temperature by multiplying by 1.44) divided by 6.25. Using this procedure, we find for the maximum in Fig. 9 at 9 K ($M_{Pb}$ derivative) an Einstein frequency of 40 cm$^{-1}$ which corresponds fairly well to the strongest peak seen in Fig. 4 for PbSe. For the Se derivative we find an Einstein frequency of 90 cm$^{-1}$, in good agreement with the Se-like peak seen in Fig. 4. Using the same procedure for Fig. 10 we find from

the $M_{Pb}$ derivative the Einstein frequency of 28 cm$^{-1}$, which also corresponds rather well to the sharp Pb-like peak of Fig. 4 for PbTe. For the $M_{Te}$ derivative we estimate an Einstein frequency of 38 cm$^{-1}$, which agrees with the maximum in the Te projection of the DOS in the corresponding vignette of Fig 4 (lowest band of PbTe). This contribution of Te to the mass derivative in the accoustic branch occurs because of the considerable contribution of the anion vibrations in this region, as displayed in Fig. 4. A similar anion contribution is negligible in the cases of PbSe and PbS.
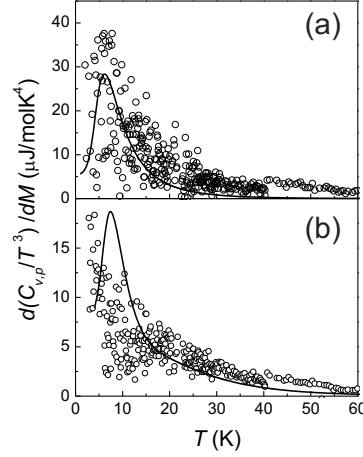


FIG. 10: Derivatives of $C_v/T^3$ of PbTe with respect to the isotopic masses of (a) Pb and (b) Te as measured using samples of different isotopic compositions, compared with *ab initio* calculations for various isotope masses with s-o interaction included.

Since most of the Te weight to the DOS is in the optical phonon region (90 cm$^{-1}$, Fig. 4 ) there should also be a corresponding peak or band in the lower vignette of Fig. 10.

The experimental data in this region scatter too much to allow observation of this peak. The calculated curve, however, should exhibit some structure in this region. Although it is hard to see in Fig. 10 it is possible to detect it if the derivative with respect to $T$ of the mass derivative is plotted. This is done in Fig. 11. In the lower vignette of this Figure, concerning the $M_{Te}$, we see indeed weak structure between 20 and 40 K which corresponds to the upper PbTe band of Fig. 4 ($90\text{cm}^{-1} \times 1.44/6.2 = 21\text{K}$).
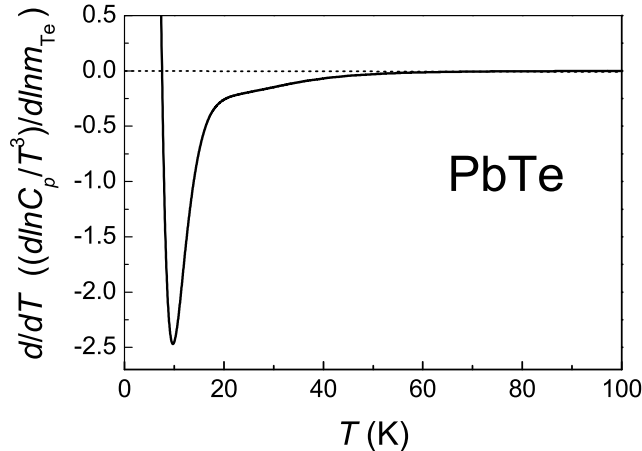


FIG. 11: (color online) Derivative with respect to $T$ of the calculated curve of Fig. 10 (lower vignette), showing a weak band in the 20-40 K region which corresponds to the Te-like band in Fig. 4 for PbTe. See text.

## VIII.   TEMPERATURE DEPENDENCE AND ISOTOPIC MASS DEPENDENCE OF $C_{V,P}/T^3$

As already mentioned, the dependence of $C_v/T^3$ and $C_p/T^3$ on isotopic mass, or more precisely the corresponding derivatives, can be obtained from the temperature dependence of $C_{v,p}/T^3$ in the case of monatomic materials. The corresponding relation for diatomic materials has been given in Eq. (2). The correctness of this equation has been demonstrated in Fig. 10 of Ref. 9 for PbS. In Fig. 12 we present one further example corresponding to PbSe.

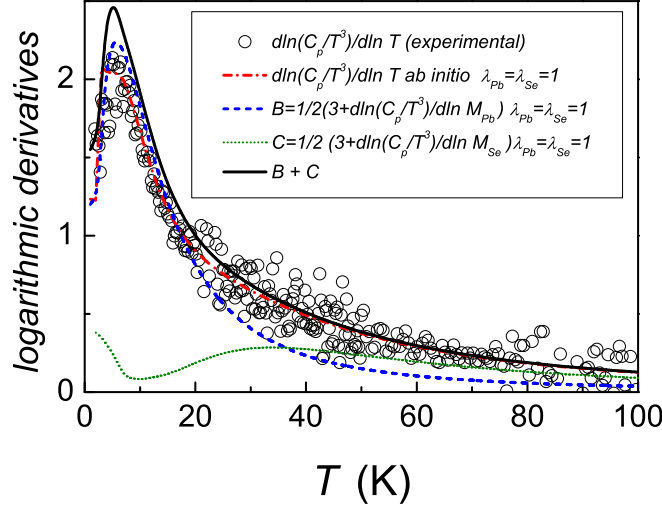The (red) dashed-dotted curve represents the derivative of the calculated logarithmic

FIG. 12: (color online) Illustration of the relationship between the temperature dependence of $C_{v,p}/T^3$ and its dependence on the isotopic masses of both constituent atoms, drawn from *ab initio* calculated data for PbSe with natural isotope abundance for Pb and Se, respectively. The (black) circles represent experimental data for the temperature dependence $(dln(C_{v,p}/T^3)/dlnT)$, the (black) solid line represent the l.h.s of Eq. (2). The other quantities are explained in the inset.

derivative of $C_v/T^3$ versus $T$. The green and blue curves represent the corresponding isotopic mass derivatives as found in Eq. (2) (obtained from the calculated data ($\lambda_{\mathrm{Pb}} = \lambda_{\mathrm{Te}} = 1$). The experimental data scatter too much to obtain meaningful results). The black curve is the sum of these derivatives. According to Eq. (2), the black and red curves should be indistinguishable. This is indeed the case for $T > 30$K. At lower temperatures the scatter of calculated and measured points becomes rather large because both $C_{v,p}$ and $T^3$ are very small. Nevertheless reasonable agreement is found. It is interesting to note that a change in the Pb mass strongly affects the $T$ dependence of $C_v/T^3$ around 5 K whereas the change in the Se mass affects that $T$ dependence in the 30-50 K region.

IX. CONCLUSIONS

We have presented theoretical and experimental investigations of some lattice properties of three lead chalcogenides (PbS, PbSe, PbTe) with rock salt struture. Because of the

presence of lead, these materials provide an excellent case study for the elucidation of the effects of spin-orbit interaction on lattice properties as derived from *ab initio* electronic structure calculations. Among other properties that have been investigated are the lattice parameters, the phonon dispersion relations, the heat capacity and their dependence on isotopic masses. The effect of spin-orbit interaction on the lattice parameters is less than 1% and can be neglected compared with other sources of computational error. Its effect on the lattice dynamics and the corresponding low temperature heat capacities is considerable. For these properties spin-orbit interaction significantly improves the agreement of theory with experiment. Because of the large scatter in the effect of isotope masses on the heat capacity, related to the small range of of isotope mass available, spin-orbit interaction does not play an important role in the comparison of theoretical and experimental data for the isotope mass dependence of the heat capacity. This dependence can be modeled on the basis of two Einstein oscillators.

We have calculated, from the *ab initio* phonon dispersion relations, the corresponding density of one-phonon states and those of two-phonon states relevant for optical spectroscopies. The latter have been compared with few extant second order Raman spectra of these materials.

* Corresponding author: E-mail r.kremer@fkf.mpg.de

[1] M. Cardona, R.K. Kremer, M. Sanati, S.K. Estreicher, T.R. Anthony, Solid State Commun. **133**, 465 2005.

[2]  A. Gibin, G. G. Devyatykh, A. V. Gusev, R. K. Kremer, M. Cardona, and H.-J. Pohl, Solid State Commun. **133**, 569 2005.

[3]  M. Sanati, S.K. Estreicher, and M.Cardona, Solid State Commun., **131**, 229 (2004).

[4]  W. Schnelle, E. Gmelin, J. Phys.: Condens. Matter **13** (2001) 6087.

[5]  J. Serrano, R. K. Kremer, M. Cardona, G. Siegle, L. E. Díaz-Sánchez, and A. H. Romero, Phys. Rev. **77**, 054303 (2008).

[6]  L. E. Díaz-Sánchez, A. H. Romero, M. Cardona, R. K. Kremer, and X. Gonze, Phy. Rev. Lett. **99**, 165504 (2007).

[7]  R. K. Kremer, M. Cardona, E. Schmitt, J. Blumm, S.K. Estreicher, S. Sanati, M. Bockowski, I. Grzegory, T. Suski, and A. Jezowski, Phys. Rev. B **72**, 075209 (2005).

[8]  J. Serrano, R.K. Kremer, M. Cardona, G. Siegle, A.H. Romero, and R. Lauck, Phys. Rev. B **73**, 094303 (2006).

[9]  M. Cardona, R. K. Kremer, R. Lauck, and G. Siegle, J. Serrano, and A. H. Romero, Phys. Rev. B **76**, 075211 (2007).

[10]  E. D. Murray, S. Fahy, D. Prendergast, T. Ogitsu, D. M. Fritz, and D. A. Reis, Phys. Rev. B **75**, 184301 (2007).

[11]  L. E. Díaz-Sánchez, A.H. Romero, X.Gonze, Phys. Rev. B **78** 104302 (2007).

[12]  X. Gonze, J.-M. Beuken, R. Caracas, F. Detraux, M. Fuchs, G.-M. Rignanese, L. Sindic, M. Verstraete, G. Zerah, F. Jollet, M. Torrent, A. Roy, M. Mikami, Ph. Ghosez, J.-Y. Raty, D.C. Allan, Comput. Mat. Sci. **25**, 478 (2002). The ABINIT code results from a common project of the Université Catholique de Louvain, Corning Incorporated, and other collaborators (http://www.abinit.org).

[13]  P. G. Etchegoin, M. Cardona, R. Lauck, R. J. H. Clark, J. Serrano, and A. H. Romero, Phys. Stat. Sol. (b) **6**, 1125 (2008).

[14]  C. Hartwigsen, S. Goedecker, and J. Hutter, Phys. Rev. B **58**, 3641 (1998).

[15]  H. J. Monkhorst and J. D. Pack, Phys. Rev. B**13**, 5188 (1976).

[16]  X. C. Gonze, Phys. Rev. B**55**, 10337 (1997).

[17]  X. C. Gonze and C. Lee, Phys. Rev. B**55**, 10355 (1997).

[18]  H. Gehlen and M. Gehlen-Keller, Ber. Deut. Chem. Ges. **73**, 1292 (1940).

[19]  A. Szczerbkow and K. Durose, Prog. Cryst. Growth Charact. Mater. 51, 91 (2005).

[20]  R. Sherwin, R. J. H. Clark, R.Lauck, and M. Cardona, Solid State Commun. **134**, 565 (2005).

[21] M. M. Elcombe, Proc. R. Soc. London, Ser. A **300**, 210 (1967).

[22] P. R. Vijayraghavan, S. K. Sinha, P. K. Iyengar, Proc. Nucl. Phys. Solid State Phys.(India) **16C**, 208 (1963).

[23] R. N. Hall and J. H. Racette, J. Appl. Phys. **32**, 2078 (1961).

[24] E. Burstein, R. Wheeler, and J. Zemel, Proc. 7th Int. Conf. on Phys. Semicond (Duno, Paris, 1964) p. 1065.

[25] G. Bauer, H. Burkhard, W, Jantsch, F. Unterleitner , A. López-Otero, in Proc. Int. Conf. on Lattice Dynamics, (Flammarion, Paris, 1978) p. 669.

[26] W. Cochran, R. A. Cowley, G. Dolling and M. M. Elcombe, Proc. Roy. Soc. London Ser.A **293**, 433 (1966).

[27] H. Preier, Appl. Phys. **20**, 189 (1979).

[28] N. Kristoffel, Sov. Physics, Sol. State **13**, 2113 (1972).

[29] E. R. Cowley, Ferroelectrics **194**, 227 (1997).

[30] Y. W. Tang and M. L. Cohen, Phys. Rev. **3**, 1254 (1970).

[31] A.L. Chang *et al.*, Chin. Phys. Lett. **17**, 606 (2000).

[32] S. V. Ovsyannikov *et al.*, J. Phys. D: Appl. Phys. **37**, 1151 (2004).

[33] Huizhen Wu, Chunfang Cao, Jianxiao Si, Tianning Xu, Hanjie Zhang, Haifei Wu, Jing Chen, Wenzhong Shen, and Ning Dai, J. Appl. Phys. **101**, 103505 (2007).

[34] F. Herman and S. Skillman, Atomic Structure Calculations (Prentice Hall, Englewood Cliffs, N.J. 1963).

[35] C. T. Anderson, J. Am. Chem. Soc. **54**, 107 (1932).

[36] D. H. Parkinson and J. E. Quarrington, Proc. Phys. Soc., London, Sect. A **67**, 573 (1954).

[37] S. N. Lykov and I. A. Chernik, Sov. Phys. Solid State **24**, 1755 (1982).

[38] A. J. Bevolo, H. R. Shanks, and D. E. Eckels, Phys. Rev. B **13**, 3523 (1976).